Hydrocarbon Emissions from In-Use Commercial Aircraft during Airport Operations

ARTICLE *in* ENVIRONMENTAL SCIENCE AND TECHNOLOGY · AUGUST 2006

Impact Factor: 5.33 · DOI: 10.1021/es051209l · Source: PubMed

6 AUTHORS, INCLUDING:

Scott Herndon
Aerodyne Research, Inc.
239 PUBLICATIONS **4,907** CITATIONS
SEE PROFILE

Todd Rogers
Columbia Basin College
17 PUBLICATIONS **427** CITATIONS
SEE PROFILE

Edward Dunlea
National Academies
82 PUBLICATIONS **3,446** CITATIONS
SEE PROFILE

W. Berk Knighton
Montana State University
151 PUBLICATIONS **2,078** CITATIONS
SEE PROFILE

Environ. Sci. Technol. **2006**, *40,* 4406−4413

Hydrocarbon Emissions from In-Use Commercial Aircraft during Airport Operations

SCOTT C. HERNDON,*,† TODD ROGERS,‡ EDWARD J. DUNLEA,§ JOHN T. JAYNE,† RICHARD MIAKE-LYE,† AND BERK KNIGHTON‡

Aerodyne Research, Inc., Billerica, Massachusetts, Montana State University, Bozeman, Montana, and Department of Earth, Atmospheric and Planetary Sciences, Massachusetts Institute of Technology, Cambridge, Massachusetts

The emissions of selected hydrocarbons from in-use commercial aircraft at a major airport in the United States were characterized using proton-transfer reaction mass spectrometry (PTR-MS) and tunable infrared differential absorption spectroscopy (TILDAS) to probe the composition of diluted exhaust plumes downwind. The emission indices for formaldehyde, acetaldehyde, benzene, and toluene, as well as other hydrocarbon species, were determined through analysis of 45 intercepted plumes identified as being associated with specific aircraft. As would have been predicted for high bypass turbine engines, the hydrocarbon emission index was greater in idle and taxiway acceleration plumes relative to approach and takeoff plumes. The opposite was seen in total NO_y emission index, which increased from idle to takeoff. Within the idle plumes sampled in this study, the median emission index for formaldehyde was 1.1 g of HCHO per kg of fuel. For the subset of hydrocarbons measured in this work, the idle emissions levels relative to formaldehyde agree well with those of previous studies. The projected total unburned hydrocarbons (UHC) deduced from the range of in-use idle plumes analyzed in this work is greater than a plausible range of engine types using the defined idle condition (7% of rated engine thrust) in the International Civil Aviation Organization (ICAO) databank reference.

Introduction

Due to the potential impact of aircraft emissions on local and regional air quality from routine airport activity, several research programs are concentrating on understanding particle and air toxic emissions. At an airport, most aircraft emissions arise from idling (at the gate and awaiting takeoff), taxiing, taking off, and landing. The characteristics of the emissions resulting from these operational modes can be very different. The factors that control the total burden the airport airshed receives from a single aircraft are the fuel-flow rate and the emission index representative of a particular engine state, along with the time spent in that state performing these various activities. It is important to characterize the relevant emission indices under all of the operational states in use at the airport in order to assess the impact of aircraft activity on local and regional air quality.

Airports represent a location where modern turbine engines are challenged with the most diverse operating conditions. Idle and takeoff are two extreme points, each with differing demands, relative to the nominal cruise operation point. Cruise is most commonly achieved in the middle and upper troposphere, but the emissions at cruise are not indicative of emissions near airports. The engine's design optimization criteria are weighted to produce the best overall economy and performance at cruise, where the bulk of the fuel on a given flight is expended, while minimizing emissions over the takeoff and landing cycle. Assessments of the impact of the airport related emissions on the local and regional scales require an inventory that accurately reflects real-world emissions (*1*−*3*).

The present study demonstrates the use of proton-transfer reaction mass spectrometry (PTR-MS) applied toward studying advected aircraft plumes at Logan airport in Boston on a single cool day (19 °C) in May 2003. The technique of using wind advected plumes and sampling the airmass rapidly is more completely described elsewhere (*4*). Exhaust plumes diluted by ambient air from individual airplanes were measured in idle, taxi, approach (or landing), and takeoff, as well as engine-start modes. The data were collected under the guidance of airport staff without interfering with airport operations. The interpretation of the measurements derived by this approach must tolerate uncertainties in the engine state, ambient conditions, and, due to the large degree of dilution for some species, instrumentation precision. Despite these limitations, this approach can give critical insight into the "real world" emission profiles for in-use jets.

In 1981 ICAO first adopted standards relating to the control of smoke and gaseous emissions (UHC, CO, and NO_x) from turbojet and turbofan engines intended for subsonic and supersonic propulsion. Each of these metrics is generally expressed in units of mass of emissions per mass of fuel, commonly (g kg^{-1}). There is a difference in the molecular mass of NO and NO_2, and in the ICAO methololgy, they are taken to be all NO_2 for this computation. Though the supersonic propulsion program has yet to see deployment in commercial airliners, these standards were developed to address aviation's contribution to air pollution in the vicinity of airports. Since the original standards were put into place, they have been modified twice, each time to reduce the permissible levels for NO_x emissions.

The findings presented here are based on fewer than 50 total plumes and, while more extensive studies are currently being analyzed, these results provide important initial perspectives on the emission magnitude and character in a downwind plume (<2 min) at an airport. This work describes the use of a proton-transfer-reaction, mass spectrometer (PTR-MS), together with other instrumentation to measure aircraft emission indices for seven hydrocarbon species at Boston Logan airport in May 2003.

Experimental Section

The use of a mobile laboratory platform to sample aviation related plumes has been documented (*4*, *5*) previously. An overview of the kinds of experiments which have been performed using the Aerodyne Mobile Laboratory has been published by Kolb et al. (*6*). Ambient air is continuously analyzed through a sample port located near the roof on the front of the truck on the driver's side and delivered to various instruments on-board the truck. Exhaust pollutant emission

* Corresponding author phone: 978-663-9500, ext. 266; fax: 978-663-4918; e-mail: herndon@aerodyne.com.
† Aerodyne Research, Inc.
‡ Montana State University.
§ Massachusetts Institute of Technology. Current address: Universisity of Colorado at Boulder, Cooperative Institute for Research in Environmental Sciences, UCB 216, Boulder, CO.

10.1021/es051209l CCC: $33.50
Published on Web 05/31/2006

ratios relative to exhaust CO_2 were determined for various gas-phase and particulate metrics by looking at the concomitant rise in the measurement of a target pollutant above background with increased CO_2. These emissions ratios can be converted to fuel-based emissions indices using above ambient CO_2 as an internal exhaust plume tracer (*7*−*9*). Though the configuration of the mobile laboratory was very different, the methodology as it applies to advected aircraft plumes is described more completely elsewhere (*4*).

Though this paper focuses on the measurements of various hydrocarbons measured using the PTR-MS, the measurements of HCHO and NO_2 emissions were performed using tunable diode laser differential absorption spectroscopy (TILDAS). Total NO_y was measured using a catalytic converter and a NO chemiluminescence instrument. Carbon dioxide, CO_2, was measured using a commercial nondispersive infrared absorption technique (Licor 6262). The PTR-MS will be described in greater detail after some brief comments about the TILDAS, NO_y, and CO_2 instruments as well as the integration into the truck sampling system.

HCHO and NO_2 Measurement. The TILDAS instrument has been described thoroughly elsewhere (*10*), and has been employed in several field measurement campaigns *(11*−*13*), but details specific to the instrument deployed in these measurements are described here. HCHO was detected using a pair of absorption lines at 1774.67 and 1774.83 cm^{-1}. Two relatively weak water lines bracket these features, and a very small water line is present in the gap between. The diode used for NO_2 was operated at approximately 1606 cm^{-1}. As operated during these measurements, the 1 s rms precision for HCHO (diode 1) was normally less than 1.2 ppbv. For NO_2 (diode 2) the 1 s rms precision was 0.8 ppbv.

The accuracy of the concentrations measured by TILDAS is determined by how well the line strengths are known. For the absorption lines used in the two instrument channels, the band strength for HCHO is known to within 7% (*14*, *15*). The bandstrength for NO_2 is known to within 4% (*16*).

CO_2 Measurement. The Licor-6262 nondispersive infrared absorption instrument detects CO_2 absorption in the 4.3 μm band. Additional details regarding its performance in this application can be found elsewhere (*4*). The measured response time of the Licor instrument to flooding the inlet tip with CO_2 free nitrogen gas during these experiments resulted in a 1/e time of 0.9 s. The Licor was calibrated with a 590 ppm CO_2 standard tank and, as deployed during this work, the absolute accuracy is estimated to be better than 6%, based on mid-IR rotation−vibration spectroscopic measurements of this standard.

NO_y Measurement. A total reactive nitrogen (NO_y) instrument from Thermo Electron Corporation (www.thermo.com) was owned and operated by MIT and located on the Aerodyne Mobile Lab. The flow to the NO_y instrument was split from the main inlet flow to the rest of the instruments on the Mobile Lab less than 2 in. from the front of the main inlet allowing as little contact time as possible with steel surfaces. Teflon tubing ($^1/_4$ in.) was used to transfer the sample flow to the NO_y converter assembly and then again from the converter to the detection chamber. The instrument employs a heated molybdenum oxide catalyst to convert both active (NO_2) and reservoir nitrogen oxide species (HONO, HNO_3, PAN, organic nitrates, particulate nitrate, etc.) to nitric oxide (NO). NO is then detected through its chemiluminescent reaction with ozone ($NO + O_3 \rightarrow NO_2 + O_2 + h\nu$). The instrument reported a total NO_y mixing ratio, corrected for pressure and temperature, every second with a maximum range of 5 ppm. The quoted detection limit is 0.4 ppb. A flow rate of 1.5 slpm was drawn through the instrument, resulting in an estimated residence time within the instrument of less than 2 s. The instrument response was calibrated against NIST-traceable standard mixtures of NO (BOC gases, 90 ppm NO in N_2, ±1%) and isopropyl nitrate (Scott-Marin gases, 10 ppm IPN in N_2, ±1%). Multiple calibrations during a previous multi-week field campaign were all within 5% of one another, indicating the relative stability of the calibrations. The dominant NO_y species in aircraft exhaust are NO and NO_2 which are typically characterized in the ICAO databank (*17*) using analytical methods (chemiluminescent measurement of NO with catalytic conversion of NO_2 to NO) equivalent to that employed here for NO_y. Based on the instrumental suite employed in this study, we cannot rule out the formation of NO_y species which are neither NO or NO_2. For the purposes of comparison with ICAO databank values, we assume that NO_y is equivalent to NO_x.

Proton-Transfer Reaction, Mass Spectrometry. The proton transfer reaction mass spectrometer (PTR-MS) used in this study was originally acquired from Ionicon Analytic GMBH and has been modified at Montana State University for deployment onboard the Aerodyne Mobile Laboratory. The PTR-MS technique has been described in detail in the review article by Lindinger et al. (*18*) and merges the concept of chemical ionization with that of the swarm technique of flow-drift tubes. Chemical ionization is based on H_3O^+ as the primary reagent ion, which does not react with the major components of clean air, but does react with most nonalkane VOCs via proton-transfer reactions. The selectivity provided by chemical ionization coupled with the sensitivity of mass spectrometry detection makes the PTR-MS a powerful analytical tool capable of rapid on-line monitoring of trace chemical species with proton affinities greater than that of water. The instrument consists of an ion source, a drift tube, a quadrupole mass analyzer, and an ion detector. A hollow cathode discharge ion source provides an intense source of H_3O^+ reagent ions. These reagent ions are collisionally equilibrated with the water vapor in the sample drift region and are injected into the drift tube through which the ambient air sample is being continuously passed at reduced pressure (typically at 2 mbar). In the drift tube, the H_3O^+ ions are pulled through the air sample by a uniform electric field applied across the length of the drift tube. The electric field imparts sufficient additional energy to the H_3O^+ ions so that they do not undergo extensive clustering with the water molecules present in the sample. In this way, bare H_3O^+ ions are transported through the drift tube without change, unless they collide with a component, R, of the air sample that has a greater proton affinity than water. In that case, R will be ionized by the proton-transfer reaction, $H_3O^+ + R \rightarrow RH^+ + H_2O$, and will be detected as RH^+ in the resulting mass spectrum.

Modifications to the original PTR-MS included replacing the original sample inlet system with the versatile high time response pressure-controlled based inlet shown in Figure 1. In addition to providing rapid sample introduction to the PTR-MS, this inlet system provides VOC-free air using heated Pt catalyst for evaluating instrumental background and for dynamic dilution of the calibrated gas standard. The inlet system is constructed from small diameter ($^1/_8$ and $^1/_{16}$ in. o.d.) PFA Teflon tubing and fittings. The critical pressure drop between the pressure controller and the main sample inlet line is provided by a stainless steel fine metering valve. This fine metering valve controls the bulk flow through the inlet and allows for variable flows from 30 to 500 sccm. The pressure controller maintains a constant 480 mbar pressure behind the metering valve. A short piece (10 in.) of 1/16 in. o.d. × 0.010 in. i.d. PFA tubing provides the necessary pressure drop between the pressure-controlled inlet line and the PTR-MS and allows about 15 sccm of the sample air stream to enter the drift tube. The total flow through the inlet under typical sampling is approximately 400 sccm. Linear velocity calculations[a] ([a]Linear velocity of the ambient gas sample equals volumetric flow rate divided by the cross sectional

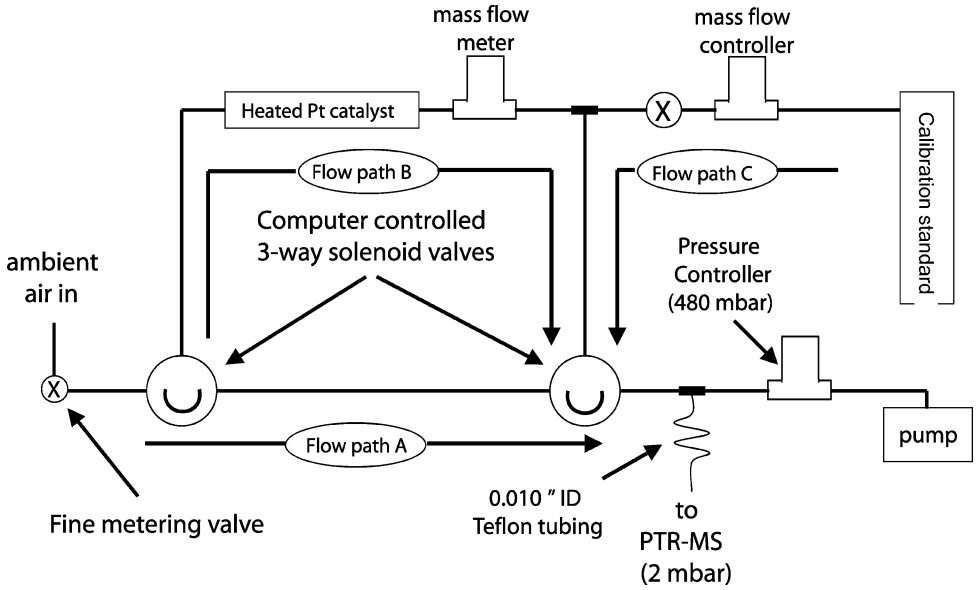

FIGURE 1. Schematic of the PTR-MS inlet system. Flow path A indicates the normal sample flow path. Typical flows of approximately 400 sccm provide short (~0.3 s) sample residence times within the inlet. Flow path B shows diversion of the ambient sample flow through the heated Pt catalyst that provides a VOC free gas stream for instrumental background measurements. Calibration experiments are accomplished when flow paths B and C are open. The extent of dilution is controlled varying the flow through flow path B by adjustment of the fine metering valve.

area of the gas line. The linear velocity of 400 sccm gas within a $^1/_8$ in. o.d. gas line exceeds 300 cm/s at 1 atm and 295 K) indicate that the sample transit time through the inlet system is short compared to the residence time in the drift tube. In this study the drift tube pressure was nominally 1.9 mbar at 295 K, and flow calculations[b] ([b]The drift tube has a diameter of 5 cm and a length of 10 cm for an estimated volume of 196 mL. The mass flow rate through the drift tube is approximately 15 sccm which corresponds to 144 mL/s at 1.9 mbar and 295 K. Assuming that the drift tube is best described as an exponential diluter the flow charactersitics are givenas $\ln(C/Co) = -(F/V)t$ which predicts a residence time ($C/Co = 0.1$) of approximately 1.6 s.) predict a sample residence time of about 1.6 s within the drift tube.

The PTR-MS data acquisition software was programmed to measure 12 masses at 0.1 s per mass along with the drift tube pressure and temperature. The acquired signals were sent to the central data processing software via dynamic data exchange (DDE) and the resulting duration of each measurement cycle was approximately 2 s. The ions monitored included the reagent ions H_3O^+ (m/z 21 ^{18}O isotope) and $H_3O^+(H_2O)$ (m/z 39 ^{18}O isotope) and 10 sample ions. Ambient air was sampled for 600 measurement cycles followed by 60 cycles of instrumental background measurement determined by diverting the sample flow through a Pt catalyst heated to 400 °C that provided a VOC free gas stream. The instrumental background is nonzero in most cases and the reported concentrations are determined as the difference between the ambient and background signals.

Determination of the concentration of a given substrate, R, from the measured ion signals is evaluated from either simple reaction kinetics (*18*) or from measured calibration response factors. In the case where the concentration of a detected substance, R, is deduced directly from the intensities (I_{RH+}) of analyte-based ions an expanded form of the standard relationship that includes the contribution of the $H_3O^+(H_2O)$ reagent ion is used:

$$\mathrm{VMR_R} = \left(\frac{I_{\mathrm{RH^+}}}{I_{\mathrm{H_3O^+}}k_c(\mathrm{H_3O^+})t + I_{\mathrm{H_3O^+(H_2O)}}k_c(\mathrm{H_3O^+(H_2O)}t}\right)\left(\frac{1}{N_{tot}}\right) \quad (1)$$

where $\mathrm{VMR_R}$ is the volumetric mixing ratio of R, N_{tot} is the total number density (molecules/mL), I_{RH^+}, $I_{H_3O^+}$, and $I_{H_3O^+(H_2O)}$ are the intensities of the respective ions in counts per seconds, t is the drift time of the reagent ions, and $k_c(H_3O^+)$ and $k_c(H_3O^+(H_2O))$ are the rate constants for the proton-transfer reaction of the respective reagent ions. The accuracy of the measurements is dependent on the uncertainty of the value of reaction rate constants and also on how well the measured $I_{H_3O^+}$ and $I_{H_3O^+(H_2O)}$ signals reflect their actual ion distributions within the drift tube (*19*). Since most simple exoergic proton-transfer reactions are known (*20*) to occur at the collision frequency, k_c can be readily calculated from either the Langevin (for nonpolar molecules) or the ADO (for molecules with significant dipole moment) theories for ion−molecule collisions (*21*). Overall, concentrations determined directly from the measured signal intensities are considered to be accurate within ± 40%. Higher quantitative accuracy can be achieved by the use of calibration standards. Calibrated responses were determined through dilution of a certified high-pressure gas mixture (Apel-Reimer) where the sensitivity factor, S_R, was determined from the slope of a 4-point dilution curve obtained by plotting $((I_{RH^+}/I_{H_3O^+} + X_R)(I_{H_3O^+(H_2O)}))$ versus $\mathrm{VMR_R}(P^2/T^2)$, a rearranged form of (*1*).

$$\mathrm{VMR_R} = \left(\frac{1}{S_R}\right)\left(\frac{I_{\mathrm{RH^+}}}{(I_{\mathrm{H_3O^+}} + X_R)(I_{H_3O^+(H_2O)})}\right)\left(\frac{T^2}{P^2}\right) \quad (2)$$

Equation 2 is intentionally shown in the same form as that of eq 1 from which it was derived. The sensitivity factor, S_R, includes all of the constant terms in eq 1 including those that define the drift time, t, and the total number density. The temperature and pressure terms originally contained within the drift time and number density remain as variables. The X_R term accounts for the difference in the reactivity between H_3O^+ and $H_3O^+(H_2O)$ reagent ions and has been determined separately by examining the humidity dependence on S_R. The calibration factors S_R and X_R used in this study are reported in Table 1. In the case of the C2-benzenes and C3-benzenes it is assumed that all of the structural isomers have the same calibration factors as their respective calibration compounds *p*-xylene and 1,2,4-trimethylbenzene. Note that the aromatic compounds do not react (*22*) with

TABLE 1. Compounds Monitored by the PTR-MS, Calibration Factors, and Limits of Detection (LD) as Operated in This Study

compound	ion (*m/z*)	S_R	X_R	LD (ppbV)[a]	LD (EI[b] g/kg fuel)
methanol	33	0.3	0.38	6.6	0.53
acetaldehyde	45	0.73	0.6	1.7	0.18
acetone	59	1.05	0.7	0.9	0.12
benzene	79	0.51	−0.4	0.9	0.17
toluene	93	0.72	−0.4	0.8	0.15
C2-benzenes	107	0.80	−0.4	1.1	0.29
C3-benzenes	121	0.75	−0.4	1.5	0.42

[a] Limit of detection based on 0.1 s *m/z* integration time. [b] Emission index (EI) limit of detection is based on a 30 ppmV change in CO_2.

$H_3O^+(H_2O)$ and so X_R for these compounds would be expected to be negative. This does not have a significant effect on our results because the calibration and sampling were made under similar reagent ion distributions. The negative value reported here compensates for the fraction of $H_3O^+(H_2O)$ originally present in the drift tube that is declustered in the expansion region between the drift tube and the mass spectrometer and is detected as H_3O^+.

The *S*/*N* has been determined directly from the scatter (3σ) in the background concentration measurements and from counting statistics as described by Hayward et al. (*23*) and de Gouw et al. (*24*) In this study, the 1σ uncertainties predicted by counting statistics were nearly identical to those experimentally determined from background concentration measurements. Limits of detection are dependent on the magnitude of the sensitivity factor and the measured background signal, and thus are different for each compound and are reported in Table 1. The limits of detection reported in Table 1 (LD) reflect the inherent variability of the short 100 ms ion intensity integration times. To temporally resolve the advected plumes under study in this work, the signal processing of the PTR-MS was matched to the flow through the drift tube. The detection limits reported in Table 1 are consistent with those reported in previous work (*25*), after accounting for differing signal averaging times.

Typically, aircraft exhaust characterization is reported as the emission index. The limit of detection expressed as an emission index is reported in Table 1. These values have been estimated via the evaluation of (*3*) assuming that ΔVMR_X is the PTR-MS limit of detection in 0.1 s and ΔVMR_{CO_2} is 30 ppmv (a typical plume encountered in this work). It should be noted that the practical limit of detection in units of effective EI will be better than those tabulated because the typical plume encounter lasts for ∼10 s.

$$\mathrm{EI\ (g/kg)} = \left(\frac{\Delta \mathrm{VMR}_x}{\Delta \mathrm{VMR}_{\mathrm{CO_2}}}\right)\left(\frac{\mathrm{MW}_x}{\mathrm{MW}_{\mathrm{CO_2}}}\right) \times 3160\ (\mathrm{g\ CO_2/kg\ fuel}) \quad (3)$$

In addition to the instruments, time-coded notes were recorded by the operators in the mobile laboratory. A sonic anemometer, located above the sampling inlet, measured wind speed and direction. A webcam automatically captured images of the upwind field of view every other second with a time code synchronized to the operator notes and the instrument data-logging. The various mixing ratios were displayed in near-real time to facilitate proper positioning of the Aerodyne Mobile Laboratory downwind from the plumes. The researchers used the real-time data analysis, typically $\Delta NO_y/\Delta CO_2$ and $\Delta HCHO/\Delta CO_2$ to assess the nature of the intercepted plumes. Working in conjunction with the airport personnel escorting the mobile laboratory on the airside, we were able to get 1−3 min downwind of aircraft in various operational modes.

Mass to Charge Ratio Assignments and Aircraft Sampling Matrix. Assignment of the neutral precursor(s) to specific ion measurements by the PTR-MS requires knowledge of the hydrocarbon speciation within the matrix and the ion products formed by the proton-transfer reaction. Compilations of the chemical composition of aircraft exhaust (*26*) and the proton-transfer reaction products for the majority of the exhaust products (*25*) allow for interpretation of the ions monitored in this study. Each of the ion assignments relevant to this study is discussed below.

Mass 33. This ion corresponds to protonated methanol. The only spectral interference to the detection of methanol is the oxygen-17 isotope of O_2^+ that is also detected at *m*/*z* 33. The contribution to O_2^+ to the ion intensity is evaluated during the instrumental background measurement process. The elevated background at *m*/*z* 33 due to O_2^+ does lead to a poorer detection limit for methanol. Methanol was not detected (<0.008 g CH_3OH kg^{-1} fuel) as an exhaust emission product in this study.

Mass 45. This ion is attributed to the presence of acetaldehyde, which is known to be a significant aircraft exhaust emission product (*26*). Proton transfer to acetaldehyde forms only the protonated molecular ion. Spectral interferences to the detection of acetaldehyde include proton transfer to ethylene glycol and propylene glycol, CO_2, and the reaction of O_2^+ and ethanol. CO_2 produces a weak response in the PTR-MS via an endothermic proton transfer reaction that occurs within the expansion region between the exit aperture of the drift tube and the entrance aperture to the quadrupole mass spectrometer and has been previously documented by de Gouw el al. (*27*). The interference due to CO_2 has been evaluated in the lab and has been found to be on the order of 1 pptV acetaldehyde equivalent per 1 ppmV CO_2 which is sufficiently small to be ignored in the present experiment. A small amount of O_2^+ (∼2% of the total ion signal) is formed within the hollow cathode ion source, and this ion can react with ethanol to form an ion at *m*/*z* 45. Ethanol, ethylene glycol, and propylene glycol have not been previously detected as components in aircraft exhaust and so the signal at *m*/*z* 45 is attributed only to the presence of acetaldehyde. Concentrations reported for acetaldehyde were deduced from measured calibration response factors.

Mass 57. This ion is expected to reflect the sum of the 3 butene isomers and acrolein. Proton transfer to all of these species is expected to produce only protonated molecular ions. Minor spectral interferences may arise (*25*) from fragmentation of proton-transfer reaction products of higher alkenes. Concentrations were deduced from (*1*) assuming an average rate constant of 2×10^{-9} ($cm^3\ s^{-1}$) for $k_c(H_3O^+)$ and $k_c(H_3O^+(H_2O)) = 0$. The concentration calculation for this species should be viewed as approximate since the actual distribution of these two species is not known and their respective reaction rate constants are quite different.

Mass 59. Three compounds are expected to contribute intensity to this ion and include acetone, propanal, and glyoxal. Proton transfer to these compounds produces primarily protonated molecular ions although acetone exhibits a small amount of fragmentation (*25*). There are no other exhaust emission components that are expected to interfere with this. Quantification of this ion signal is based on an acetone calibration response factor and the reported concentration should be considered as a lower limit to the sum of these species as the reaction rate constant for glyoxal (*28*) (1.3×10^{-9} ($cm^3\ s^{-1}$)) is smaller than that of acetone and propanal.

Mass 61. This ion is often attributed (*24*) to the presence of acetic acid. Acetic acid was not previously reported as an aircraft exhaust emission product and was not detected in this study.

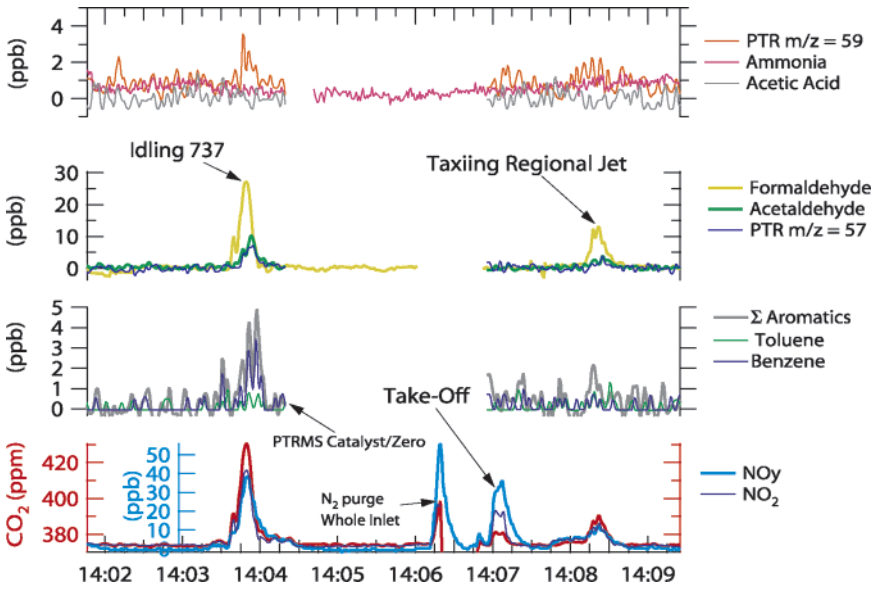

FIGURE 2. Time series for multiple species at Logan Airport. Figure shows data collected as wind advected plumes were sampled at Logan Airport. All scales are in ppbv, except for the CO_2 data (ppmv). The figure shows three fully resolved plumes: a taxiing 737 just before 14:04, a takeoff plume at 14:07, and an idling regional jet at ~14:08. See text for additional discussion.

Mass 79. This ion is predominately formed via a proton-transfer reaction with benzene. The proton-transfer reaction products of some of the higher order monosubstituted benzenes such as ethylbenzene and propylbenzene fragment within the PTR-MS to produce ion at m/z 79. Relative to benzene, the presence of these other alkylbenzenes in aircraft exhaust is expected to be small (*26*) and the total intensity measured at m/z 79 is therefore attributed to benzene.

Mass 93. This ion reflects the presence of toluene. There are no known or expected interferences to measurement of toluene in this matrix.

Mass 107. Several compounds contribute intensity to this ion which includes the three xylene isomers, ethylbenzene, and benzaldehyde. Normally the C2-benzene isomers dominate this ion signal although there are indications that in aircraft exhaust benzaldehyde (*26*) may be a significant contributor to the ion intensity at this mass. Concentrations have been calculated using *p*-xylene as the calibration standard which assumes that all of these species have the same response factors. The validity of this assumption seems quite reasonable for the C_8H_{10} isomers but is uncertain for benzaldehyde as this compound has been observed (*25*) to have an unusually low response factor relative to its calculated reaction rate constant.

Mass 121. There are six C_9H_{12} isomers and up to three C_8H_8O isomers that can contribute intensity to this ion. Formally, this ion is referred to as reflecting the C3-benzenes although there is no independent hydrocarbon speciation data to confirm this assumption. Concentrations have been calculated using 1,2,4-trimethylbenzene as the calibration standard which assumes that all of these species have the same response factors. The validity of this assumption is not unreasonable for the C_9H_{12} isomers (*25*), but is uncertain relative to the oxygenated isomers.

Results and Discussion

A time series showing several of the species measured in this study is shown in Figure 2. The lowest panel shows CO_2 in red, which is employed as the dilution tracer in this work. Over the 7-minute period depicted in this figure, four distinct aircraft plumes are observed. A zero air purge at 14:06:20 suspended the sampling and the plume that was interrupted was not analyzed. In the time series depicted by Figure 2, one takeoff and two idle plumes have been analyzed. On the lowest panel the cyan-blue represents total NO_y and the thin dark blue represents the NO_2 mixing ratio. The panel second from the bottom contains the aromatic compounds. The panel third from the bottom shows the results for formaldehyde, acetaldehyde, and $m/z^+ = 57$. Finally, the uppermost panel shows $m/z^+ = 59$, acetic acid, and ammonia.

Figure 2 shows several interesting features. First, the plume with the greatest NO_y to CO_2 ratio is the plume labeled 'takeoff' based on the video record. All other organic species shown in the figure have no observed increased concentrations for the takeoff plume. This is in contrast to the idle plume, which shows increased formaldehyde, acetaldehyde, aromatics, and elevated levels of the species at $m/z^+ = 57$ and 59. Elevated hydrocarbon emissions for the taxi plumes relative to takeoff plumes would be anticipated, based on the International Civil Aviation Organization (ICAO) data bank sheets for unburned hydrocarbons (UHC) for all modern turbine engines (*17*). The aircraft in question, in Figure 2 visually identified as an idling 737, was likely fitted with GE CFM56 engines. The model of the engines on the taxiing regional jet are unknown, but this figure illustrates that after accounting for dilution, the magnitude of the hydrocarbon emission indices vary from one engine to another.

Comparison of EI(NO_y) to ICAO(NO_x). The measured NO_y emission index for the plume labeled takeoff in Figure 2 is 5.9 ± 0.8 ppb NO_y ppm^{-1} CO_2 or 19.5 ± 3.9 g (kg fuel)$^{-1}$. This plume originated from a 737 most likely using CMF56 engines. The average value of the 100% power (takeoff) NO_x emission index for all models of CMF56 taken from the ICAO emissions data bank ranges from 17 to 31 g (kg fuel)$^{-1}$. Without an exact engine model, however, no additional comparative interpretation can be done for this single plume. The general level of agreement between measurements and the tabulated data bank in this example and other NO_y takeoff plumes lends confidence that this methodology may be applied to speciated hydrocarbon emission indices for the idle and taxiway plumes.

The analysis of all plumes sampled in this study is summarized in Table 2. The number of plumes at each category represents a maximum number of potentially analyzed plumes. Occasionally, the tunable diode laser system was off-line and, as a result, five plumes were missed. At different times, the internal catalytically generated-zero-air took the PTR-MS off-line and six plumes were not sampled.

TABLE 2. NO_y and Selected Hydrocarbon Results

	LD[a] (g kg^{-1})	idle	taxiway acceleration	approach[b] (touchdown)	takeoff
plumes		13	10	6	15
species		median $\pm$ 1σ (g kg^{-1})	median $\pm$ 1σ (g kg^{-1})	median (g kg^{-1})	median $\pm$ 1σ (g kg^{-1})
NO_y	0.03	2 $\pm$ 1.9	10 $\pm$ 9	13	19 $\pm$ 9
HCHO	0.1	1.1 $\pm$ 0.4	0.7 $\pm$ 0.2	0.2	0.04 $\pm$ 0.2
acetaldehyde	0.2	0.4 $\pm$ 0.3	0.3 $\pm$ 0.8	0.09	0.12 $\pm$ 0.3
$m/z^+ = 57$	0.4	0.5 $\pm$ 0.4	0.4 $\pm$ 0.4	$-$0.4	$-$0.04 $\pm$ 0.8
$m/z^+ = 59$	0.1	0.2 $\pm$ 0.4	0.21 $\pm$ 0.5	0.3	0.04 $\pm$ 0.4
benzene	0.1	0.3 $\pm$ 0.3	0.22 $\pm$ 0.6	0.1	0.05 $\pm$0.1
toluene	0.1	0.2 $\pm$ 0.3	0.18 $\pm$ 0.5	0.2	0 $\pm$ 0.4
C2$-$benzene	0.2	0.4 $\pm$ 0.7	0.15 $\pm$ 0.5	0.2	0.1 $\pm$ 0.3
C3$-$benzene	0.3	0.3 $\pm$ 0.6	0 $\pm$ 1	0.1	0.08 $\pm$ 0.8

[a] The calculated limit of detection (LD) is based on the instrument 1-s rms divided by the typical plume strength. In this work the typical plume encountered was 30 ppm CO_2. [b] An insufficient number of plumes of this nature were sampled to calculate a meaningful standard deviation within the sample. The variability of EI in this category was qualitatively similar to that observed in the takeoff plumes.

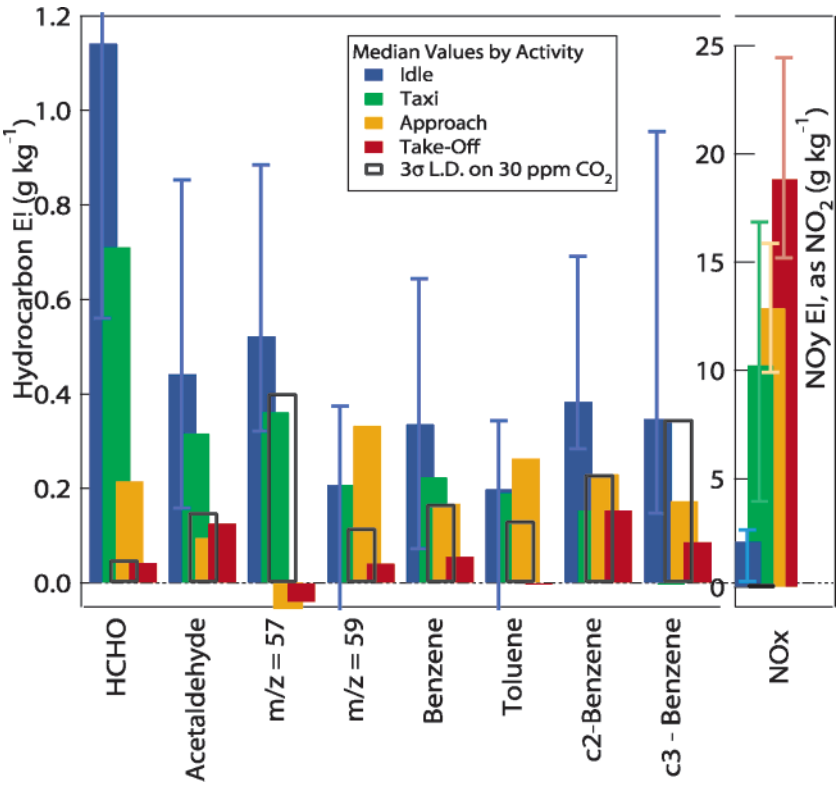

FIGURE 3. Selected hydrocarbon and NO_y results by activity. The median values of the emission index for each of idle, taxi, approach, and takeoff are plotted for selected hydrocarbons and total NO_y. The whiskers on each NO_y activity and on the hydrocarbon idle results represent the 25th to 75th quartiles. The black open bars are a visual representation of the detection limit estimated using the procedure described in the text.

The table reports the median EI value for each of the idle, taxiway acceleration, approach, and takeoff plumes. Along with each median value, one standard deviation of the mean is reported. Though the sample sizes are too low for this reported deviation to be meaningful, it should give some insight into the observed variability for the result. This also may be compared to the LD, included as the first column. It should be noted that the plumes encountered which are called out as "Approach" in Table 2 (for comparisons to ICAO) are more indicative of the air to ground switch-over as the aircraft is landing. Accordingly, this header is subtitled "Touchdown" to reflect the ambiguous and possibly variable nature of the throttle setting in the engines for these plumes.

Figure 3 captures the overall trends evident in the data presented in Table 2. The aircraft exhaust resulting from engine idle and taxiway acceleration generally contain greater concentrations of hydrocarbons than the exhaust during landing and takeoff. This observation is qualitatively consistent with the ICAO databank values for hydrocarbon emissions at idle relative to takeoff. To compare these selected hydrocarbon measurements and the UHC data in the ICAO databank, these two disparate datasets must be put on an equivalent basis.

Comparison of Hydrocarbon EI with ICAO. The ICAO UHC emissions data are tabulated in the databank as g CH_4 per kg fuel. When the median values of the measured speciated HCs in Table 2 (direct mass Emission Indices) are summed and converted to equivalent carbon methane, the emission index for the idle plumes is 2.9 g (kg fuel)$^{-1}$ for the subset of species detected in this work. In this study, the composition of the aircraft traffic measured at Logan Airport wasregional jets, 737s, MD88s, and 757s. For comparison purposes, the mix of engines sampled is assumed to be composed of CF34, AE 3007, CFM-56, JT8D, and RB211 class engines. This can be justified only via anecdotal knowledge of the engines typically installed on the visually identified

airframes. By employing a plausible mixture of the relevant engines for the air traffic sampled, the 25th to 75th percentile of the ICAO UHC emissions data represents 3.8−5.1 g of methane per kg fuel. This suggests that 50−75% of the total methane equivalent hydrocarbons were detected and speciated in this work when compared to the ICAO UHC data.

There are few reports of speciated hydrocarbon measurements and inventories to compare to the present results. We can address the issue of what fraction of total hydrocarbons should have been observed by consulting data from the European Environment Agency's EMEP COMAIRE program (*29*). The average speciated hydrocarbon emissions during a landing−takeoff (LTO) cycle for a representative mixture of commercial aircraft operating in Europe is well summarized in Table 2 of Pison et al. (*1*). The EMEP COMAIRE data represent an entire LTO cycle and are averaged over all commercial aircraft in use in Europe. This tabulation can provide a useful second point of comparison with two assumptions. First, that the differences in hydrocarbon speciation between the two airframe/engine sets are small. Second, that the emissions at idle dominate the nature of the speciation or that speciated hydrocarbon measurements are relatively fixed regardless of the engine's state. Assuming these are valid assumptions, the hydrocarbons measured in this work indexed to the values tabulated in Table 2 of Pison et al. indicates that this work should have observed ∼40% of the total hydrocarbon emissions in methane equivalent g per kg fuel.

The qualitative agreement between these approaches (ICAO and EMEP/COMAIRE) to extrapolating the measurements to a total hydrocarbon emission index is encouraging, despite the assumptions made in identifying appropriate engines to include in the average and the categorical application of the EMEP COMAIRE speciation. Using the 40% estimate for the fraction of measured HCs, together with the results from Table 2 in this work, 2.9 g (kg fuel)$^{-1}$, the total UHCs can be estimated as 7.2 g (kg fuel)$^{-1}$. This is somewhat greater than the ICAO-derived range of 3.8−5.1 g (kg fuel)$^{-1}$ for total UHCs. While within a factor of 2 or so, more direct and quantitative comparisons would be possible with more complete identification of the emitting aircraft engine. Spicer et al. (*24*) found the UHC emission index to be 9.1 g kg^{-1} for a CFM56 at idle. This compares more favorably to the projection based on these measurements. In future work, the tail number for each aircraft must be recorded in order to compare the measured emission index to the certification value for the specific engine.

Anticipating the ability to make such detailed comparisons in the future, there are difficulties associated with making a direct comparison of the magnitudes of the emissions in Table 2 and those tabulated in ICAO. ICAO defines the idle condition to be 7% of rated thrust where this study sampled plumes, which were either at "ground idle" (an engine state which is below 7% of rated thrust for most engines designed in the last 30 years) or were performing taxiway accelerations. In similar work, the NO_x emission index was observed to vary significantly between ground idle and taxiway acceleration (*4*). A similar difference exists for takeoffs, in that many aircraft take off at "derated thrust" or less than 100% of rated thrust. So actual operation does not match the nominal tabulated ICAO thrust condition and direct comparisons between actual operations and ICAO tabulated values may have complications. Measured data from actual operations, however, are invaluable for determining emissions budgets and such comparisons to ICAO data can be used to evaluate how well the ICAO data can be used to represent airport emissions budgets as is currently done. The Emissions Dispersion Modeling System (EMDS), developed and maintained by the Federal Aviation Administration, uses ICAO as well as other information from engine manufacturers in its emissions inventory (*30*, *31*).

TABLE 3. Comparison of Hydrocarbon Emission Indices for Idle Plumes

species/HCHO	Spicer et at. (26) CFM-56 (g per g HCHO)	this work various engines (g per g HCHO)
acetaldehyde/HCHO	0.35	0.26
(acrolein+ butene)/HCHO	0.36[a]	0.25
(acetone + propanal + glyoxal)/HCHO	0.24	0.09
benzene/HCHO	0.14	0.11
toluene/HCHO	0.05	0.06
C2-benzenes/HCHO	0.09[b]	0.09

[a] The (acrolein + butene)/HCHO ratio for Spicer et al. (*26*) was computed using the results for 1-butene, 2-*cis*-butene, and acrolein and converting each with the appropriate number of carbon atoms. [b] The C2-benzene/HCHO ratio for Spicer et al. (*26*) was computed using results for each of the xylene isomers, ethyl benzene, and benzaldehyde.

Comparison to Speciated Hydrocarbon Measurements. To quantify the speciation of emitted hydrocarbons, Spicer et al. (*26*) measured a wide variety of individual hydrocarbons in the exhaust of a TF-39 and a CFM56 engine using whole air canister samples for off-line analysis by various GC techniques while the engine was running at ground idle, and 30% and 80% of rated thrust. Similarly, Anderson et al. (*32*) collected whole air samples 10 m downstream from an RB-211 at the Experiment to Characterize Aircraft Volatile Aerosol and Trace-Species Emissions (EXCAVATE).

The results of Anderson et al. (*32*) indicate substantial differences in the speciation of various hydrocarbon families (alkenes vs alkanes) with increasing engine pressure ratio (EPR) or increasing fraction of rated thrust. They found that the total NMHC emission index decreases by a factor of 75 from EPR 1.03 to EPR 1.15, which is similar to the trend observed in Table 2 and Figure 3 of this work. Measurement of the continuous particulate emission index in the Anderson et al. work showed substantial variability over the course of a single power condition and the authors suggest that a single grab sample may not be representative of the average hydrocarbon emission index at that power setting.

To compare the results in Table 2 to the work of Spicer et al., the variability between engines must be addressed. As discussed previously, the magnitude of the hydrocarbon emission index can be very different from one engine to the next. We postulate that the relative abundances of specific hydrocarbons may have less variability from one engine to the next. In this work, we propose the use of the formaldehyde emission index to normalize varying hydrocarbon emissions magnitudes (between aircraft engines) to focus the comparison on the nature of the relative speciation. Formaldehyde is present as one of the most dominant hydrocarbon concentrations and is thus a valuable reference hydrocarbon species. Another potential choice would be ethylene, however it was not measured with sufficient detection sensitivity during this work. Results from this normalization are presented in Table 3. The median value for the formaldehyde emission index in this work compares very favorably to the Spicer et al. result for the CFM56 engine (1.1 and 1.2 g kg^{-1}, respectively).

The comparison of specific hydrocarbon emission indices relative to that of formaldehyde shows very good qualitative agreement (Table 3). As discussed previously, two of the PTR-MS signal masses represent multiple compounds. To compare these results to the GC-FID results in Table 3, some species have been summed as noted.

Despite several assumptions, particularly regarding the ensemble of airframe/engine combinations sampled, this work indicates that the effective hydrocarbon emission index

for idling in-use aircraft may be greater than that tabulated for idle at 7% rated thrust in the ICAO databank by 40−90%. This disparity is likely due to the range of thrust levels encountered in this work to be lower than 7%. Future studies which employ this methodology must note the specific engine in order to make direct comparisons to the tabulated quantities in ICAO.

Acknowledgments

The authors gratefully acknowledge the assistance of Flavio Leo, Aviation Planning Manager, and Vincent Cardillo, Airport Operations Manager, at The Massachusetts Port Authority. We would like to thank Gregg Fleming of Volpe National Transportation Systems Center for assistance. This work was funded in part by the MCMA field measurement program within the Integrated Program on Urban, Regional, and Global Air Pollution at Massachusetts Institute of Technology and the Centers for Atmospheric and Environmental Chemistry and Aero-Thermodynamics at ARI.

Literature Cited

(1) Pison, I.; Menut, L. Quantification of the impact of aircraft traffic emissions on tropospheric ozone over Paris area. *Atmos. Environ.* **2004**, *38*, 971−983.

(2) Yu, K. N.; Cheung, Y. P.; Chueng, T.; Henry, R. C. Identifying the impact of large urban airports on local sir quality by nonparametric regression. *Atmos. Environ.* **2004**, *38*, 4501−4507.

(3) Unal, A.; Hu, Y.; Chang, M. E.; Odman, M. T.; Russel, A. G. Airport related emissions and impacts on air quality: Application to the Atlanta International Airport. *Atmos. Environ.* **2005**, *39*, 5787−5798.

(4) Herndon, S. C.; Shorter, J. H.; Zahniser, M. S.; Nelson, D. D. J.; Jayne, J. T.; Brown, R. C.; Miake-Lye, R. C.; Waitz, I. A.; Silva, P.; Lanni, T.; Demerjian, K. L.; Kolb, C. E. NO and NO_2 emission ratios measured from in-use commercial aircraft during taxi and takeoff. *Environ. Sci. Technol.* **2004**, *38*, 6078−6084.

(5) Herndon, S. C.; Onasch, T., B.; Frank, B. P.; Marr, L. C.; Jayne, J. T.; Canagaratna, M. R.; Grygas, J.; Lanni, T.; Anderson, B. E.; Worsnop, D. R.; Miake-Lye, R. C. Particulate emissions from in-use commercial aircraft. *Aerosol Sci. Technol.* **2005**, *39*, 799−809.

(6) Kolb, C. E.; Herndon, S. C.; McManus, J. B.; Shorter, J. H.; Zahniser, M. S.; Nelson, D. D.; Jayne, J. T.; Canagaratna, M. R.; Worsnop, D. R. Mobile laboratory with rapid response instruments for real-time measurements of urban and regional trace gas and particulate distributions and emission source characteristics. *Environ. Sci. Technol.* **2004**, *38*, 5694−5703.

(7) Anderson, B. E.; Cofer, W. R.; Bagwell, D. R.; Barrick, J. D.; Hudgins, C. H.; Brunke, K. E. Airborne observations of aircraft aerosol emissions I: Total nonvolatile particle emission indices. *Geophys Res. Lett.* **1998**, *25*, 1689−1692.

(8) Fahey, D. W.; Keim, E. R.; Boering, K. A.;. Brock, C. A; Wilson, J. C.; Jonsson, H. H.; Anthony, S.; Hanisco, T. F.; Wennberg, P. O.;Miake-Lye, R. C.; Salawitch, R. J.; Louisnard, N.; Woodbridge, E. L.; Gao, R. S.; Donnelly, S. G.; Wamsley, R. C.; Del Negro, L. A.; Solomon, S.; Daube, B. C.; Wofsy, S. C.; Webster, C. R.; May, R. D.; Kelly, K. K.; Loewenstein, M.; Podolske, J. R.; Chan, K. R. Emission measurements of the Concorde Supersonic aircraft in the lower stratosphere. *Science* **1995**, *270*, 70−74.

(9) Schäfer, K.; Jahn, C.; Sturm, P.; Lechner, B.; Bacher, M. Aircraft emission measurements by remote sensing methodologies at airports. *Atmos. Environ.* **2003**, *37*, 5261−5271.

(10) McManus, J. B.; Kebabian, P. L.; Zahniser, M. S. Astigmatic mirror multiple pass absorption cells for long pathlength spectroscopy. *Appl. Opt.* **1995**, *34*, 3336−3348.

(11) Zahniser, M. S.; Nelson, D. D.; McManus, J. B.; Kebabian, P. L. Measurement of trace gas fluxes using tunable diode laser spectroscopy. *Philos. Trans., R. Soc. London A* **1995**, *351*, 371−382.

(12) Horii, C. V.; Zahniser, M. S.; Nelson, D. D.; McManus, J. B.; Wofsy, S. C. Nitric Acid and Nitrogen Dioxide Flux Measurements: a New Application of Tunable Diode Laser Absorption Spectroscopy; Application of Tunable Diode and Other Infrared Sources for Atmospheric Studies and Industrial Process Monitoring. *SPIE Proc.* **1999**, *3758*, 152−161.

(13) Li, Y.; Schwab, J.; Roychowdhury, U.; Ren, X.; Brune, W.; Karcher, R.; Zahniser, M. S.; Nelson, D. D. J.; Herndon, S. C.; Demerjian, K. L. Intercomparison of formaldehyde, sulfur dioxide and nitrogen dioxide measurement techniques during the PMTACS-NY Summer 2002 Campaign at Whiteface Mountain, 2003.

(14) Herndon, S. C.; Yongquan, L.; Nelson, D. D.; Zahniser, M. S. Determination of line strengths for selected transitions in the nu2 band relative to the nu1 and nu5 bands of H2CO. *JQSRT* **2005**, *90*, 207−216.

(15) Volkamer, R. Comparison of the absorption cross-section of HCHO in the UV and IR spectral ranges. Personal Communication; 2005.

(16) Smith, M. A. H.; Rinsland, C. P.; Fridovich, B.; Rao, K. N. Intensities and Collision Broadening Parameters From Infrared Spectra. In *Molecular Spectroscopy: Modern Research*; Academic Press: New York, 1985; Chapter 3.

(17) ICAO, International Civil Aviation Organization *Aircraft Engine Emissions DataBank*. 2006. http://www.caa.co.uk/docs/702/introduction-05102004.pdf.

(18) Lindinger, W.; Hansel, A.; Jordan, A. On-line monitoring of volatile organic compounds at pptv levels by means of proton-transfer-reaction mass spectrometry (PTR-MS) - Medical applications, food control and environmental research, *Int. J. Mass Spectrom.* **1998**, *173*, 191−241.

(19) Warneke, C.; van der Veen, C.; Luxembourg, S.; de Gouw, J. A.; Kok, A. Measurements of benzene and toluene in ambient air using proton-transfer-reaction mass spectrometry: calibration, humidity dependence and field intercomparison. *Int. J. Mass Spectrom.* **2001**, *207*, 167−182.

(20) Harrison, A. G. *Chemical Ionization Mass Spectrometry*; CRC Press Inc.: Boca Raton, FL, 1992.

(21) Su, T.; Bowers, M. T. *Classical Ion−Molecule Collision Theory In Gas-Phase Ion Chemistry*; Academic Press: New York, 1979.

(22) Spanel, P.; Smith, D. Reactions of Hydrated Hydronium Ions and Hydrated Hydroxide Ions with Some Hydrocarbons and Oxygen-Bearing Organic Molecules. *J. Phys. Chem.* **1995**, *99*, 15551−15556.

(23) Hayward, S.; Hewitt, C. N.; Sartin, J. H.; Owen, S. M. Performance Characteristics and Applications of a Proton Transfer Reaction-Mass Spectrometer for Measuring Volatile Organic Compounds in Ambient Air. *Environ. Sci. Technol.* **2002**, *36*, 1554−1560.

(24) de Gouw, J. A.; Goldan, P. D.; Warneke, C.; Kuster, W. C.; Roberts, J. M.; Marchewka, M.; Bertman, S. B.; Pszenny, A. A. P.; Keene, W. C. Validation of proton transfer reaction-mass spectrometry (PTR-MS) measurements of gas-phase organic compounds in the atmosphere during the New England Air Quality Study (NEAQS) in 2002. *J. Geophys. Res.* **2003**, *108*, D21.

(25) Warneke, C.; de Gouw, J. A.; Kuster, W. C.; Goldan, P. D.; Fall, R. Validation of Atmospheric VOC Measurements by Proton-Transfer- Reaction Mass Spectrometry Using a Gas-Chromatographic Preseparation Method. *Environ. Sci. Technol.* **2003**, *37*, 2494−2501.

(26) Spicer, C. W.; Holdren, M. W.; Riggin, R. M.; Lyon, T. F. Chemical composition and photochemical reactivity of exhaust from aircraft turbine engines. *Ann. Geophys.* **1994**, *12*, 944−955.

(27) de Gouw, J. A.; Warneke, C.; Karl, T.; Eerdekens, G.; van der Veen, C.; Fall, R. Sensitivity and specificity of atmospheric trace gas detection by proton-transfer-reaction mass spectrometry. *Int. J. Mass Spectrom.* **2003**, *223*, 365−382.

(28) Zhao, J.; Zhang, R. Y. Proton transfer reaction rate constants between hydronium ion (H_3O^+) and volatile organic compounds. *Atmos. Environ.* **2004**, *39*, 2177−2185.

(29) European Environment Agency. EMEP/CORINAIR Emission Inventory Guidebook; EEA Group 08; 2004; http://reports.eea.eu.int/EMEPCORINAIR4/en/page002.html.

(30) Federal Aviation Administration. Emissions and Dispersion Modeling System (EDMS); 2006; http://www.faa.gov/about/office_org/headquarters_offices/aep/models/edms_model/.

(31) Fleming, G. Personal communication.

(32) Anderson, B. E.; Blake, D. R.; McEachern, M. Hydrocarbon Emissions from a Modern Commercial Airliner. *NASA Technical Memorandum*; 2003; Appendix B, 8.

Received for review June 24, 2005. Revised manuscript received March 27, 2006. Accepted April 28, 2006.

ES051209L